


Structure and dynamics of the radical cation of ethane arising from the Jahn-Teller and Pseudo-Jahn-Teller effects

Journal Article

Author(s):

Jacovella, Ugo; Stein, Christopher J.; Grütter, Michel; Freitag, Leon; Lauzin, Clément; [Reiher, Markus](#) ; Merkt, Frédéric

Publication date:

2018-01-14

Permanent link:

<https://doi.org/10.3929/ethz-b-000207636>

Rights / license:

[In Copyright - Non-Commercial Use Permitted](#)

Originally published in:

Physical Chemistry Chemical Physics 20(2), <https://doi.org/10.1039/C7CP06907C>

Funding acknowledgement:

172620 - Precision measurements with cold molecules: Rydberg states, ions and photoionization (SNF)

This article may be downloaded for personal use only. Any other use requires prior permission of the author and The Royal Society of Chemistry.

The following article appeared in *Phys. Chem. Chem. Phys.* **20**, 1072-1081 (2018) and may be found at <http://dx.doi.org/10.1039/C7CP06907C>.

Cite this: DOI: 10.1039/xxxxxxxxxx

Structure and dynamics of the radical cation of ethane arising from the Jahn-Teller and Pseudo-Jahn-Teller effects

U. Jacovella^a, C. J. Stein^a, M. Grütter^a, L. Freitag^a, C. Lauzin^a, M. Reiher^a and F. Merkt^a

Received Date

Accepted Date

DOI: 10.1039/xxxxxxxxxx

www.rsc.org/journalname

The pulsed-field-ionization zero-kinetic-energy photoelectron spectrum of C_2H_6 has been recorded in the region of the adiabatic ionization threshold. The partially rotationally resolved spectrum indicates the existence of several vibronic states of $C_2H_6^+$ with less than 600 cm^{-1} of internal excitation. The analysis of the rotational structures assisted by *ab initio* calculations enabled the determination of the adiabatic ionization energy of C_2H_6 and the investigation of the structure and dynamics of $C_2H_6^+$ at low energies. The ground state of $C_2H_6^+$ is found to be a 2A_g state of diborane-like structure with strongly mixed $(a_{1g})^{-1}$ and $(e_g)^{-1}$ configurations. The vibrational structure reveals the importance of large-amplitude nuclear motions involving the diborane distortion modes, the C–C stretching motion, and the internal rotation at elongated C–C distances. The spectrum is analyzed in the light of the information obtained in earlier studies of $C_2H_6^+$ by *ab initio* quantum chemistry, EPR spectroscopy and photoelectron spectroscopy.

1 Introduction

The radical cation of ethane, $C_2H_6^+$, is a simple open-shell hydrocarbon. Its low-lying electronic states, $\tilde{X}^+ {}^2E_g$, $\tilde{A}^+ {}^2A_{1g}$ and $\tilde{B}^+ {}^2E_u$, can be qualitatively interpreted as arising upon removal of an electron out of one of the three outer-valence-shell orbitals e_g (C–H bonds), a_{1g} (C–C bond) and e_u (C–H bonds) of the $(1a_{1g})^2 (1a_{2u})^2 (2a_{1g})^2 (2a_{2u})^2 (1e_u)^4 (3a_{1g})^2 (1e_g)^4 \tilde{X}^+ {}^1A_{1g}$ ground electronic state of ethane, respectively. The CH_3 moieties are staggered in ethane, which has an equilibrium structure of D_{3d} point-group symmetry and high barriers for internal rotation.¹

The \tilde{X}^+ ground electronic state of $C_2H_6^+$ is doubly degenerate for structures of D_{3d} symmetry and therefore subject to the Jahn-Teller (JT) effect^{2,3} along vibrational modes of a_{1g} and e_g symmetry. The e_g modes split the 2E_g into a ground A_g and an excited B_g component and distort the structure from D_{3d} to C_{2h} symmetry. The structure and dynamics of $C_2H_6^+$ is further complicated by the small energy difference between the $3a_{1g}$ and $1e_g$ orbitals of ethane, which implies a close energetic proximity of the \tilde{X}^+ and \tilde{A}^+ states.

Removal of an electron from the e_g orbital of ethane (depicted in Fig. 1) followed by JT distortion of the 2E_g state along the e_g CH_3 -rocking mode leads to an equilibrium structure of C_{2h} point-group symmetry similar to that of diborane, with two in-plane H atoms on long C–H bond forming a CCH angle of only $\sim 82^\circ$ and four out-of-plane H atoms on shorter C–H bonds and forming

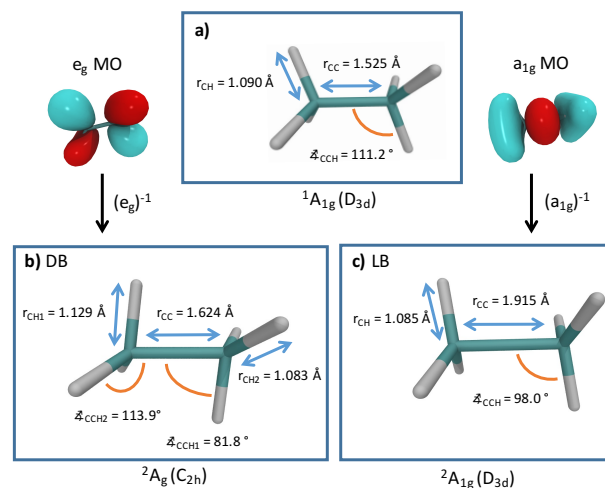


Fig. 1 Equilibrium structures of the $\tilde{X}^+ {}^1A_{1g}$ electronic ground state of C_2H_6 (a), the diborane-like isomer of $C_2H_6^+$ (b), and the long-bond isomer of $C_2H_6^+$ (c) (see Section 3 for details). The e_g and a_{1g} outer-valence-shell orbitals of C_2H_6 that play a role in the interpretation of the photoelectron spectrum of C_2H_6 are drawn schematically on either side of panel (a).

large CCH angles, see, e.g., Refs. 4–13 and Fig. 1b. This structure is referred to as the diborane-like isomer (called DB structure or DB isomer below). Removal of an electron from the a_{1g} orbital (also depicted in Fig. 1) leads to a second structure, of D_{3d} sym-

^a Laboratory of Physical Chemistry, ETH Zurich, CH-8093 Zurich, Switzerland

metry and ${}^2A_{1g}$ electronic character, characterized by a long C–C bond^{4–13} (see Fig. 1c). This structure is hence referred to as the long-bond (LB) isomer.

The A_g component of the E_g state and the A_{1g} state interact through a pseudo Jahn-Teller (PJT) effect and their electronic configurations are mixed at distorted geometries. Whereas early calculations predicted the LB isomer of $C_2H_6^+$ to be more stable,^{14,15} most calculations since the work of Richartz *et al.*^{4,16} agree that the DB isomer is the more stable structure.^{5–13} There are three equivalent structures corresponding to both the DB and the LB isomers, which can be interconverted by a large-amplitude pseudo-rotational motion and internal rotation, respectively (see Fig. 7 below). Ioffe and Shaik⁷ concluded that the lowest energy path to interconvert two DB C_{2h} structures is through a $D_{3d} {}^2A_{1g}$ structure. Sulzbach *et al.*¹⁰ came to a similar conclusion and identified the interconversion path to be a change from the $C_{2h} {}^2A_g$ DB-like minimum to the D_{3d} long-bond structure followed by internal rotation around the C–C bond and a change back to another of the three C_{2h} DB-like structures.

Ab initio quantum-chemical calculations have also been used in combination with model vibronic-coupling Hamiltonians based on the Köppel-Domcke-Cederbaum (KDC) approach to vibronic coupling problems¹⁷ to characterize the JT and PJT effects in $C_2H_6^+$ as observed by photoelectron spectroscopy.^{11–13} Venkatesan and Mahapatra¹¹ considered linear and quadratic JT effects in the $\tilde{X}^+ {}^2E_g$ state and the PJT effect coupling the \tilde{X}^+ and \tilde{A}^+ states to calculate the intensity distribution of the photoelectron spectrum for comparison with the He I photoelectron spectrum reported in Ref. 18. They found qualitative agreement after shifting the calculated spectrum by +0.1 eV.¹¹ Kumar *et al.*¹² pointed at the need to include bilinear coupling terms (anharmonic coupling terms coupling different modes), higher-order coupling terms and the PJT coupling to the $\tilde{B}^+ {}^2E_u$ state. A weakness of this approach in treating systems subject to large JT distortions is the expansion of the potentials around the equilibrium structure of the neutral molecule, because the expansion may not converge rapidly. To overcome this problem, Lee *et al.*¹³ calculated the photoelectron spectrum of ethane in the 11–15 eV region using linear and full quadratic JT and PJT Hamiltonians with up to 70 billion direct-product basis functions, in what they described as the largest time-independent KDC-model calculation ever performed. They found good to excellent agreement of the calculated photoelectron spectrum with the experimental spectrum of Baker *et al.*,¹⁹ except perhaps in the immediate vicinity of the adiabatic ionization threshold (see their Figure 2b). Understanding the photoelectron spectrum of ethane in this region is, however, crucial to fully characterize the structure and dynamics of $C_2H_6^+$.

Iwasaki and coworkers^{20,21} concluded from their studies of the EPR spectrum of $C_2H_6^+$ in solid matrices of SF_6 at 4.3 K and 77 K that the ground state of $C_2H_6^+$ has a C_{2h} DB-like structure, with the electron-spin density localized on the two in-plane C–H bonds. They indeed observed the hyperfine structure as a triplet at 4.2 K, which evolved into a septet at 77 K. They interpreted this spectral change as being caused by the rapid matrix-induced interconversion (pseudorotation) of the C_{2h} DB-like structures,

which renders all six protons equivalent on the EPR measurement timescale. Their conclusions were strengthened by a subsequent investigation of the effects of partial deuteration on the EPR spectra,²² which indicated the preferential occupation of the in-plane bond by H atoms and of the out-of-plane bonds by D atoms through zero-point-energy effects. Such effects make the three C_{2h} DB-like structures energetically inequivalent and hinder the large-amplitude pseudorotation. The situation is thus similar to that encountered in the radical cation of methane, which has a fluxional ground state in CH_4^+ but is a rigid rotor in $CH_2D_2^+$, where the protons (deuterons) occupy the long (short) bonds.^{23–29} This similarity of behavior between CH_4^+ and $C_2H_6^+$ is not accidental because (i) $C_2H_6^+$ can be thought of as a methane cation in which an H atom has been replaced by a methyl group, and (ii) both molecules are subject to a very strong JT effect in their electronic ground state.

In the present article, we report on a measurement of the photoelectron spectrum of C_2H_6 in the vicinity of the adiabatic ionization threshold at high spectral resolution using the technique of pulsed-field-ionization zero-kinetic-energy (PFI-ZEKE) photoelectron spectroscopy,³⁰ with the goals of a) determining the adiabatic ionization energy of C_2H_6 , and b) studying the structure and dynamics of $C_2H_6^+$ at low energies. The lowest bands we observed are located below the first band seen in the He I photoelectron spectrum,^{18,19,31–34} in a region where the photoelectron signal is extremely weak, making the recording of rotationally resolved spectra very challenging. The spectra turned out to also be challenging to assign and their interpretation proposed here is complementary to previous analyses of the JT effect.^{11–13}

2 Experimental procedure

The experiments were carried out using the techniques of PFI-ZEKE photoelectron spectroscopy³⁰ and the laser system and spectrometer described in Ref. 35. The region around the adiabatic ionization threshold of the $\tilde{X}^+ \leftarrow \tilde{X}$ photoionizing transition of C_2H_6 was accessed using tunable vacuum-ultraviolet (VUV) laser radiation generated by resonance-enhanced four-wave mixing. Overview spectra of the wavenumber ($\tilde{\nu}_{VUV}$) region between 92 600 cm^{-1} and 93 350 cm^{-1} were recorded using VUV radiation produced by difference-frequency mixing $\tilde{\nu}_{VUV} = \tilde{\nu}_1 + \tilde{\nu}_2 - \tilde{\nu}_3$ in Ar, exploiting the $3p^5 4p'[1/2]_0 \leftarrow 3p^6 ({}^1S_0)$ two-photon resonance ($\tilde{\nu}_1 + \tilde{\nu}_2 = 108\,722.65 \text{ cm}^{-1}$) of Ar, which was accessed using the main emission line of a F_2 excimer laser ($\tilde{\nu}_1 = 63\,439.3222(40) \text{ cm}^{-1}$)³⁶ and the frequency-tripled output of a commercial Nd:YAG-pumped pulsed dye laser ($\tilde{\nu}_2 = 45\,283.33 \text{ cm}^{-1}$). The VUV wavenumber was changed over the desired spectral range by scanning the wavenumber $\tilde{\nu}_3$ of another pulsed dye laser between 15 375 and 16 125 cm^{-1} . Tunable VUV radiation in the same spectral range was also generated by resonance-enhanced sum-frequency mixing ($\tilde{\nu}_{VUV} = 2\tilde{\nu}'_1 + \tilde{\nu}'_2$) in Xe using the $5p^5 6p[1/2]_0 \leftarrow 5p^6 [{}^1S_0]$ two photon resonance ($2\tilde{\nu}'_1 = 80\,118.98 \text{ cm}^{-1}$) by tuning the wavenumber $\tilde{\nu}'_2$ of a pulsed dye laser between 12 475 and 13 225 cm^{-1} . This second method of generating VUV radiation led to much larger VUV intensities beyond 92 800 cm^{-1} but suffered from an intensity hole between 92 650 and 92 750 cm^{-1} , which prevented the recording of PFI-

ZEKE photoelectron spectra in this region. The VUV wavenumber was calibrated with an accuracy of 0.3 cm^{-1} by recording optogalvanic spectra of Ar and Ne while scanning the dye-laser wavenumbers. The repetition rate of the pulsed laser was 16.67 Hz for the experiments relying on the F_2 excimer laser and 25 Hz otherwise. In both cases, the bandwidth of the VUV laser radiation was 0.5 cm^{-1} .

The VUV radiation was separated from the laser radiation of other wavenumbers using a vacuum monochromator equipped with a dispersion grating, as described in Ref. 35, and was directed in the photoexcitation region of the spectrometer, where it crossed a supersonic beam of a mixture of Ar and C_2H_6 in a pressure ratio of 10:1. The photoionization spectra were recorded by extracting the photoions using a pulsed field of 200 V/cm delayed by $1 \mu\text{s}$ with respect to the VUV laser pulse. The PFI-ZEKE photoelectron spectra were obtained by monitoring the pulsed field ionization of very high Rydberg states located in narrow, well-defined energy ranges below the successive rovibrational ionization thresholds of C_2H_6 as a function of the VUV wavenumber. The strength of the electric field pulses was adjusted to achieve the best compromise between high resolution and high sensitivity. To obtain the positions of the field-free ionization thresholds, the shifts induced by the field-ionization were corrected for as explained in Ref. 37. The photoelectron signal near the adiabatic ionization threshold was very weak and many recordings collected under identical experimental conditions had to be added to improve the signal-to-noise ratio of the photoelectron spectra.

3 Computational methods and results

The dependence of the energy and electronic character on the C-C bond length r_{CC} is crucial to understand the structure and dynamics of C_2H_6^+ at low energies.^{7,10} Fig. 2 illustrates this aspect for the electronic energy obtained with multiconfigurational complete-active-space second-order perturbation theory (CASPT2)³⁸ as a function of r_{CC} obtained from constrained complete-active-space self-consistent-field (CASSCF)^{39–42} structure optimizations. A full valence active space with 13 electrons in 14 orbitals was applied in combination with a def2-TZVP atomic orbital basis set⁴³ for the calculation of the doublet ground state.

The dashed black line represents results obtained without any point-group symmetry restriction but constraining r_{CC} , whereas D_{3d} symmetry was enforced to obtain the red circles, which correspond to a state of A_{1g} symmetry. The latter restrictions were enforced in a Z-matrix, where only the six identical CCH angles and six identical CH bond distances were optimized for each value of r_{CC} . The electronic-energy curves in Fig. 2 describe the main structural features of C_2H_6^+ , in particular the two minima corresponding to the DB and LB isomers (black dashed line) and the fact that the LB isomer is of almost pure $(a_{1g})^{-1}$ character, as can be concluded from the energy equality of the dashed black curve and the red circles in the range $r_{\text{CC}} > 1.85 \text{ \AA}$. The figure also illustrates that the A_{1g} $(a_{1g})^{-1}$ state is the ground state at large C-C distances whereas the A_g component of the Jahn-Teller-split E_g $(e_g)^{-1}$ state is the ground state at short C-C distances. This is confirmed by the weights of the dominant CASSCF determinants

that reveal an almost pure $(a_{1g})^{-1}$ character for the LB isomer and a mixture of $(a_{1g})^{-1}$ and $(e_g)^{-1}$ character for the DB isomer.

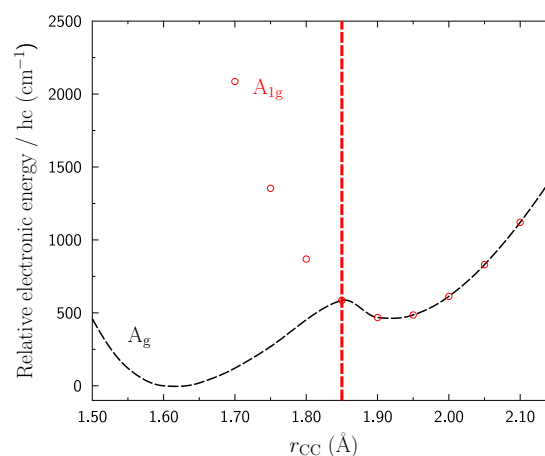


Fig. 2 Relaxed CASPT2/CASSCF potential-energy surface scan along the C-C stretch coordinate r_{CC} . The dashed black curve was obtained by constraining only the r_{CC} coordinate whereas D_{3d} symmetry was enforced to calculate the red circles (see text for details).

In order to obtain a better value for the energy difference ΔE between the DB and LB equilibrium structures, we carried out explicitly correlated,^{44,45} partially spin-restricted coupled-cluster calculations with singles and doubles excitations and perturbative inclusion of triples excitations (RCCSD(T)).^{46,47} We refined the two CASSCF equilibrium structures with numerical gradients and monitored the convergence with respect to the basis-set size by repeating all calculations with explicitly correlated valence double-zeta (VDZ-F12), triple-zeta (VTZ-F12), and quadruple-zeta (VQZ-F12) basis sets along with corresponding auxiliary basis sets.⁴⁸ The final values were obtained with the VQZ-F12 basis set and all calculations were carried out with the Molpro suite of *ab initio* programs.⁴⁹

The refined structures of the DB and LB isomers are depicted in panels b and c of Fig. 1, respectively, where they are compared to the equilibrium structure of the neutral ground state (panel a) calculated in the same manner. Coupled-cluster calculations were also performed to determine the adiabatic ionization energy, $E_{\text{I,ad}}$, which corresponds to the energy difference between the ground vibrational levels of the DB isomer of C_2H_6^+ and the neutral ground state. $\frac{E_{\text{I,ad}}}{hc} = 92850 \text{ cm}^{-1}$ ($=11.512 \text{ eV}$) was obtained using Eq.(1)

$$E_{\text{I,ad}} = E_{\text{I,BO}} + E_0(\text{C}_2\text{H}_6^+, \text{DB}) - E_0(\text{C}_2\text{H}_6), \quad (1)$$

where $E_{\text{I,BO}}/hc = 94170 \text{ cm}^{-1}$ is the energy difference between the minima of the relevant potentials, and $E_0(\text{C}_2\text{H}_6^+, \text{DB})/hc = 15100 \text{ cm}^{-1}$ and $E_0(\text{C}_2\text{H}_6)/hc = 16420 \text{ cm}^{-1}$ are the corresponding zero-point vibrational energies calculated in the harmonic approximation. The value of the adiabatic ionization energy is in agreement, within the expected accuracy of our calculation, with the value of $11.52(4) \text{ eV}$ reported by Lee *et al.*¹³ (see Table 1 below). The energy difference between the DB and the

LB isomer is determined to be 250 cm^{-1} using

$$\Delta E = \Delta E_{\text{BO}} + E_0(\text{C}_2\text{H}_6^+, \text{LB}) - E_0(\text{C}_2\text{H}_6^+, \text{DB}) \quad (2)$$

with $\Delta E_{\text{BO}}/(hc) = 340\text{ cm}^{-1}$ and $E_0(\text{C}_2\text{H}_6^+, \text{LB})/(hc) = 15010\text{ cm}^{-1}$.

Finally, coupled-cluster calculations were carried out to determine the difference in Born-Oppenheimer energy of C_2H_6^+ in the A_g state at the equilibrium structures of neutral C_2H_6 and of the DB isomer of C_2H_6^+ . We find a value of 8897 cm^{-1} , which indicates a very strong JT effect.

4 Experimental results

4.1 Overview of the photoelectron spectrum of C_2H_6 near the adiabatic ionization threshold of the $\tilde{X}^+ \leftarrow \tilde{X}$ photoionizing transition.

The photoionization and PFI-ZEKE photoelectron spectra of ethane in the vicinity of the adiabatic ionization threshold of the $\tilde{X}^+ \leftarrow \tilde{X}$ ionizing transition are displayed in panels a and b of Fig. 3, respectively. The PFI-ZEKE photoelectron spectrum consists of three main bands, labeled 1–3, with partially resolved rotational structure, and of a very weak band located halfway between Bands 2 and 3.

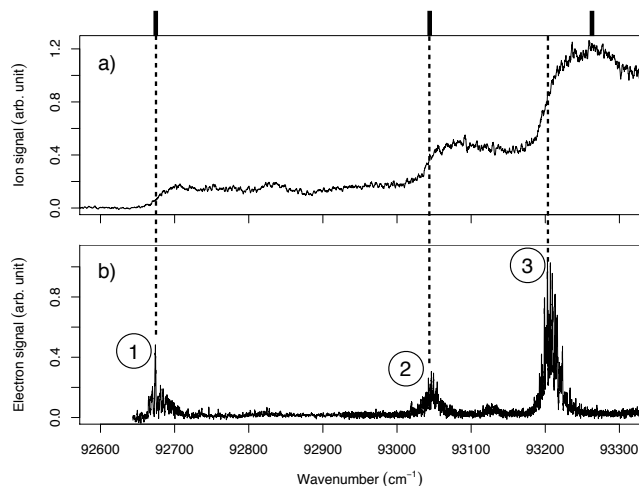


Fig. 3 Photoionization (a) and PFI-ZEKE photoelectron (b) spectra in the region of the adiabatic ionization threshold of the $\tilde{X}^+ \ ^2E_g \leftarrow \tilde{X} \ ^1A_{1g}$ photoionizing transition of C_2H_6 . The thick marks given at the top of the figure indicate the positions predicted by the simple effective tunneling model presented in Section 5.

The spectrum was recorded under conditions where hardly any clusters could be detected in the supersonic beam. We therefore attribute all three main bands to C_2H_6 . This attribution is supported by the general appearance of the photoionization spectrum obtained by monitoring the C_2H_6^+ ion yield after mass selection with a time-of-flight spectrometer. This spectrum has no measurable intensity below the lowest band of the PFI-ZEKE photoelectron spectrum, with center at about 92680 cm^{-1} , but several clear stepwise intensity increases at positions coinciding with the three main bands of the photoelectron spectrum. The coincidence of sharp steps in a photoionization spectrum with bands

of the corresponding photoelectron spectrum indicates that autoionization does not significantly contribute to the photoionization yield, as is the case, e. g., when Rydberg states belonging to series converging on excited ionic levels rapidly decay by predissociation.⁵⁰ The photoionization and photoelectron spectra thus reveal the existence of at least two vibronic levels of C_2H_6^+ located within 600 cm^{-1} of the lowest observed cationic level.

The large structure changes expected upon ionization of ethane as a result of the strong JT distortion predicted theoretically make the identification of the band origin and the determination of the adiabatic ionization energy of the $\tilde{X}^+ \leftarrow \tilde{X}$ photoionizing transition of C_2H_6 challenging. There is indeed no guarantee that the lowest band observed in the photoelectron spectrum corresponds to the transition to the vibrationless ground ionic state. Moreover, the large change of structure may favour the observation of hot bands in the photoelectron spectrum.

The only vibrational level of C_2H_6 that may be significantly populated in the supersonic expansion is the 4^1 level located $\sim 290\text{ cm}^{-1}$ above the ground state.¹ The separations of the lowest observed band of the photoelectron spectrum from the next ones, i.e., 370 cm^{-1} for Band 2 and 530 cm^{-1} for Band 3, are different from the vibrational wavenumber of the 4^1 ground-state level so that we can rule out that Band 1 is a hot band. Experiments in which we changed the expansion conditions of the supersonic beam by changing the nozzle stagnation pressure, the carrier gas, and the relative timing of the nozzle opening time and laser pulse consistently gave the same relative intensities for Bands 1–3 and support this conclusion.

Although we cannot absolutely rule out that Band 1 corresponds to a transition to an excited cationic state, we consider this possibility to be unlikely. No photoionization signal could indeed be detected below Band 1 (see Fig. 3a) despite considerable efforts invested to detect one. Moreover, all high-level *ab initio* calculations of the adiabatic ionization energy of ethane,^{7,13} including our own (see Section 3) give values located within 250 cm^{-1} of Band 1.

Further information on the photoionization of ethane and on the structure of C_2H_6^+ was obtained from the partially resolved rotational structures of Bands 1–3, which are displayed on an enlarged scale in panels a–c of Fig. 4, respectively. Whereas the intensity distribution of Band 1 is dominated by a sharp central line at 92675 cm^{-1} , reminiscent of a Q-type branch in an optical spectrum with weaker lines on either side, Bands 2 and 3, which have a very similar overall appearance, are characterized by broader intensity distributions. These observations suggest that the ionic level accessed through Band 1 has a different vibronic symmetry and/or a different structure than those accessed through Bands 2 and 3.

4.2 Rotational structure of the first bands of the photoelectron spectrum of the $\tilde{X}^+ \leftarrow \tilde{X}$ transition.

To model the rotational structure of the bands depicted in Fig. 4, we follow the general procedure outlined in Refs. 50,51. In the present case, we first deduce the effective rotational Hamiltonian and molecular symmetry group appropriate to describe the rota-

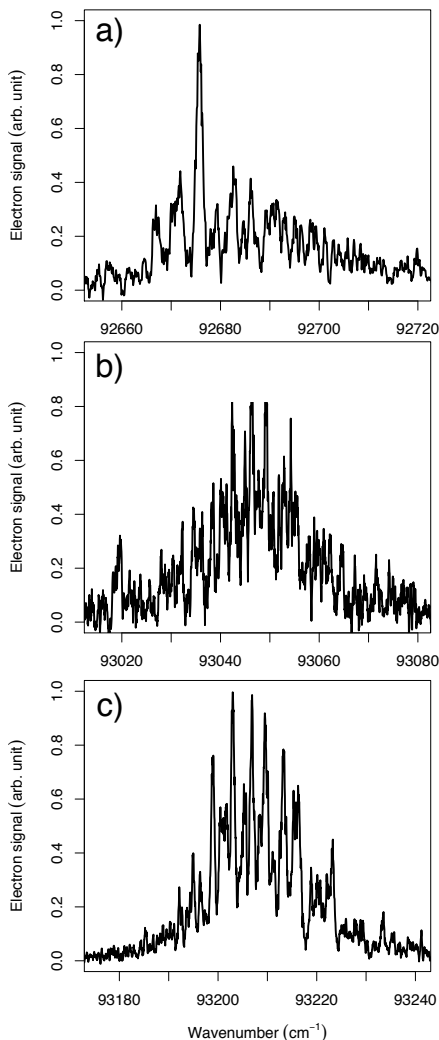


Fig. 4 a–c) Rotational structures of the three main bands, labeled 1–3 in Fig. 3, respectively, of the PFI-ZEKE photoelectron spectrum of the $\bar{X}^+ \leftarrow \bar{X}$ photoionizing transition of C_2H_6 .

tional structure of $C_2H_6^+$ from the knowledge of the structure and dynamics of $C_2H_6^+$ acquired in previous experimental and *ab initio* quantum-chemical studies.^{4–15,18–20,22,31–34,52,53} We then derive rovibrational photoionization selection rules taking into account the possible vibronic symmetries of the ionic levels observed experimentally and apply them considering restrictions imposed by the character of the molecular orbitals involved in the photoionization of C_2H_6 and the JT effect in $C_2H_6^+$. Finally, we model the rotational intensity distributions of selected bands of the photoelectron spectrum and compare them to the structures observed experimentally, and so restrict the range of possible assignments. This procedure relies on a qualitative, simplified single-electron description of the electronic structure and the photoionization process.

The relevant cationic structures are either symmetric-top or near-symmetric-top molecules (see Fig. 1) for which the differences between the values of the B and C rotational constants are too small to be observed at the resolution of our experiment. The rotational structures of the photoelectron spectra are thus mod-

elled using the standard expression for rotational level energies of a prolate symmetric top ($A > B \simeq C$)

$$\frac{E_{N^{(+)}K^{(+)}}}{hc} = B^{(+)}N^{(+)}(N^{(+)} + 1) + (A^{(+)} - B^{(+)})K^{(+)^2} \quad (3)$$

for both C_2H_6 and $C_2H_6^+$, where $N^{(+)}$ and $K^{(+)}$ are the quantum numbers associated with the rotational angular momentum vector and its projection on the top axis, which is the a axis.

The relative intensities of the rotational lines are calculated using the expression^{50,51}

$$I_{NK \rightarrow N^+K^+} \propto \rho'' \sum_{|\lambda''| \leq \ell''} \frac{1}{2\ell'' + 1} Q(\ell'') B_{\ell'', \lambda''}^{(\alpha)}, \quad (4)$$

where the angular factor $Q(\ell'')$ is given by

$$Q(\ell'') = (2N^+ + 1) \left[\begin{pmatrix} N^+ & \ell'' & N'' \\ -K^+ & \lambda'' & K'' \end{pmatrix} \right]^2. \quad (5)$$

ρ'' represents the product of the nuclear-spin-statistical weight (i.e., 8 for $K = 0$, even- J levels; 16 for $K = 0$, odd- J levels; 20 for $K = 3n \pm 1$ levels with $n = 0, 1, 2, \dots$; and 24 for $K = 3n$ levels with $n = 1, 2, \dots$) and the Boltzmann factors of the vibronic ground-state levels of C_2H_6 . $B_{\ell'', \lambda''}^{(\alpha)}$ is a factor that includes radial transition integrals connecting the molecular orbital (MO) out of which the electron is ejected and the photoelectron partial wave. ℓ'' and λ'' in Eqs. (4) and (5) represent the orbital angular momentum and projection quantum numbers, respectively, resulting from a single-center expansion of the MO out of which the electron is ejected, i.e., either the e_g or the a_{1g} valence orbitals of C_2H_6 depicted in Fig. 1. Inspection of these orbitals and taking the quantization axis to lie along the top axis leads to the conclusion that the a_{1g} has dominant d_{z^2} ($\ell''=2, \lambda''=0$) and weaker s ($\ell''=0, \lambda''=0$) character and that the e_g orbital has d_{xz} or d_{yz} ($\ell''=2, \lambda''=1$) character.

The result of this procedure is illustrated in Fig. 5, which compares the rotational structure of the origin band (Band 1, Fig.5a) with the rotational structures predicted on the basis of different hypotheses concerning the ground-state structure, as is now discussed in detail.

Assuming that the origin band corresponds to a transition to the ground state of the long-bond isomer of D_{3d} structure (see Fig. 1c), A_{1g} electronic symmetry and a_{1g} vibrational symmetry implies ionization out of the a_{1g} MO of C_2H_6 . From the s ($\ell''=0, \lambda''=0$) and d_{z^2} character ($\ell''=2, \lambda''=0$) of this orbital, the dominant transitions are predicted to be those following the selection rules $\Delta N = N^+ - N'' = 0, \pm 1, \pm 2$ and $\Delta K = 0$. If the internal rotation is assumed to be hindered, the rotational structure (see Fig. 5b) is predicted to consist of a dominant sharp Q-type ($\Delta N = 0$) branch with weaker and broader $\Delta N = \pm 1$ and $\Delta N = \pm 2$ branches on either side. The $B=C$ rotational constant of the long-bond isomer (0.51 cm^{-1} from the structure depicted in Fig. 1c) is reduced compared to that of the neutral ground state (0.66 cm^{-1}) so that the $\Delta N = 1$ and $\Delta N = 2$ branches have band heads on the high wavenumber side and the $\Delta N = -1$ and -2 branches have a gradually decreasing intensity distribution on the

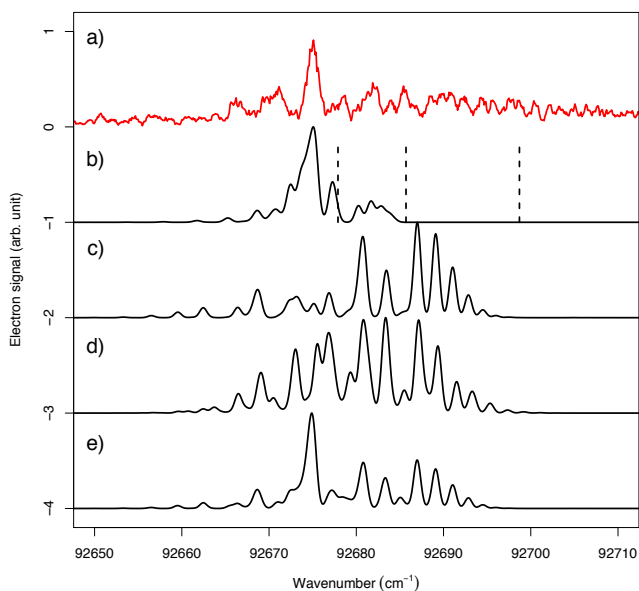


Fig. 5 a) Rotational structure of the origin band of the PFI-ZEKE photoelectron spectrum of the $\tilde{X}^+ \leftarrow \tilde{X}$ ionizing transition of C_2H_6 and model calculations of the contributions expected for b) a transition to the LB isomer following ejection out of the a_{1g} MO, c) a transition to the DB isomer following ejection out of the e_g MO, d) a transition to a hypothetical ground state of E_g vibronic symmetry with DB-like structure, and e) a transition to the A_g ground state of the DB isomer assuming a 5 % s and a 25 % d_{z^2} contribution from $(a_{1g})^{-1}$ ionization and a 70 % contribution from $(e_g)^{-1}$ ionization (see text for details).

low-wavenumber side, in contrast to the experimental spectrum. Assuming free internal rotation of the methyl groups of the LB isomer would lead to additional sharp structures separated from the main Q-type branch by $A^+K_i^2$ ($K_i = 1, 2, 3, \dots$) at the positions marked by dashed vertical lines in Fig 5b, which is also incompatible with the experimental spectrum. We thus rule out that Band 1 corresponds to a transition to the LB isomer.

Assuming that the origin band corresponds to a transition to the DB isomer of C_{2h} equilibrium structure resulting from the JT effect in the E_g cationic state implies ionization out of the e_g MO of C_2H_6 (This orbital is depicted in Fig. 1). This assumption requires one to either work in the C_{2h} group if the three equivalent C_{2h} structures are separated by high pseudorotation barriers or in the D_{3d} group if the pseudorotation splitting into a tunneling pair of levels of A_{1g} and E_g vibronic symmetry is resolved. In either case, the d_{xz} or d_{yz} character of the e_g MO (see Fig. 1) implies $|\lambda''| = 1$ in Eq. (5), which excludes a Q-type branch but favors $\Delta K = \pm 1$ and $\Delta N = \pm 1, \pm 2$ branches. Because the B^+ and C^+ rotational constants of the DB-like structure are almost identical, the spectra we predict for the A_g (C_{2h}) and A_{1g} (D_{3d}) structures (see Fig. 5c) are almost identical but lack the sharp central line characteristic of the experimental spectrum. The overall width of the rotational distribution, however, corresponds well to that of the experimental spectrum. The spectrum calculated for a ground state of E_g (D_{3d}) vibronic symmetry has an even broader distribution (see Fig. 5d) and is also incompatible with the experimental

spectrum. We therefore rule out that Band 1 corresponds to a transition to a state formed by a pure $(e_g)^{-1}$ ionization.

From these considerations, we conclude that a contribution from $(a_{1g})^{-1}$ ionization is necessary to account for the sharp Q-type branch observed experimentally but that rotational constants similar to those of the DB isomer are needed to account for the overall extent of the band. Both conclusions indicate that the ground state of $C_2H_6^+$ results from the JT and PJT effects and is a state of A_g electronic and A_g vibronic symmetry (C_{2h}) with a mixed electronic configuration consisting of A_g $(e_g)^{-1}$ and $(a_{1g})^{-1}$ contributions and an equilibrium structure similar to that of the DB-like isomer. To obtain the model spectrum presented in Fig. 5e, we assumed a 5 % s and 25 % d contributions of the $(a_{1g})^{-1}$ component and a 70 % contribution of the $(e_g)^{-1}$ component and the rotational constants $A^+ = 2.60 \text{ cm}^{-1}$ and $B^+ \simeq C^+ = 0.59 \text{ cm}^{-1}$ that are close to those of the DB-like isomer depicted in Fig. 1b. The overall appearance of the experimental spectrum is well reproduced by this model spectrum, which enables us to attribute the central sharp line of the experimental spectrum to a $\Delta N = 0$ Q-type branch arising from the $(a_{1g})^{-1}$ ionization contribution. This attribution enables us in turn to determine the adiabatic ionization energy $E_{I,ad}$ of ethane to be $92675(2) \text{ cm}^{-1}$ or $11.4902(2) \text{ eV}$. Table 1 compares this new value with earlier experimental and theoretical values of $E_{I,ad}$.

Method	$E_{I,ad} / \text{eV}$	Ref.
ST4CCD/6-311G**	11.48	[7]
QCISD(T)/6-311G**	11.51	[7]
HEAT	11.52(4)	[13]
RCCSD(T)/VQZ-F12	11.512	this work
He I	11.49	[31]
He I	11.56	[19]
PFI-ZEKE	11.4902(2)	this work

Table 1 Summary of calculated and measured adiabatic ionization energies ($E_{I,ad}$) of C_2H_6 .

A similar procedure, applied to Bands 2 and 3, leads to the conclusion that, in both cases, the ionic state has E_g (D_{3d}) vibronic symmetry and that the electronic state possesses mixed A_{1g} ($(a_{1g})^{-1}$ ionization) and A_g ($(e_g)^{-1}$ ionization) character. Because both bands have a similar rotational structure (see Fig. 4), only Band 3 is depicted in Fig. 6 (panel a) because of its stronger overall intensity and the resulting higher signal-to-noise ratio. The main contributions to the overall intensity distribution of this band are depicted in panels b and c of Fig. 6, which show respectively, the spectra predicted for the $(e_g)^{-1}$ component with selection rules $\Delta N = \pm 1, \pm 2$ and $\Delta K = \pm 1$ as discussed above, and for the $(a_{1g})^{-1}$ component with the selection rules $\Delta N = 0, \pm 1, \pm 2$ and $\Delta K = 0$. This latter contribution is crucial to explain the feature indicated by the dashed vertical line in Fig. 6. Unexpectedly, we also had to include a weak $|\Delta K| = 2$ contribution (panel d) to the spectrum, without which it is not possible to account for the two features marked by dotted lines. This contribution may originate from rovibrational interactions or internal rotation. Unfortunately, the overall weakness of the bands prevented us from

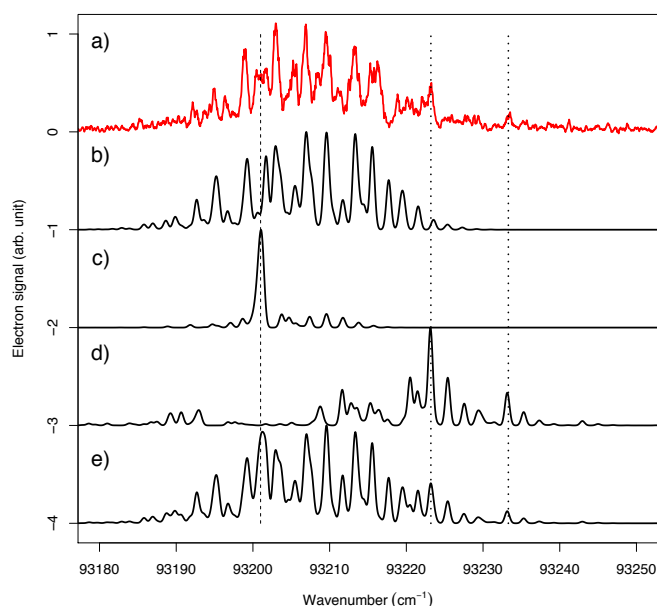


Fig. 6 a) Rotational structure of Band 3 of the PFI-ZEKE spectrum of C_2H_6 and model calculations of the contributions predicted for b) the $(e_g)^{-1}$ component, c) the $(a_{1g})^{-1}$ component, d) the $|\Delta K| = 2$ contribution, and e) a weighted sum of these contributions (see text for details).

recording spectra at higher resolution and better signal-to-noise ratio to clarify the origin of this contribution. The spectrum depicted in the bottom panel of Fig. 6 represents the sum of these three contributions weighted with the factors of 0.7 b), 0.2 c) and 0.1 d), respectively, and can be regarded to be in good agreement with the experimental spectrum, especially if one considers its weakness and low signal-to-noise ratio.

Table 2 summarizes our attributions of Bands 1–3 and the molecular constants we used to model their rotational structures. Given that we could not reach a quantitatively perfect agreement between experimental and simulated spectra, some uncertainty concerning these assignments persists. The low wavenumbers of

	Band 1	Band 2	Band 3
T / cm^{-1}	92 675(2)	93 042(2)	93 202(2)
T^+ / cm^{-1}	0	367	527
A^+ / cm^{-1}	2.60	2.58	2.58
$B^+ \simeq C^+ / \text{cm}^{-1}$	0.59	0.61	0.61
Γ_{ve}	A_g	E_g	E_g

Table 2 Origins (T) of the main three bands of the photoelectron spectrum of C_2H_6 near the adiabatic ionization threshold and corresponding ion term values (T^+), rotational constants and vibronic symmetries.

the two excited vibronic levels of $C_2H_6^+$ corresponding to Bands 2 and 3 suggest the importance of large amplitude motions in $C_2H_6^+$ already at low energies, presumably taking place on a multidimensional subspace of the potential-energy surface. Their attribution to specific vibrational levels would necessitate calculations of the vibrational motion on a multidimensional potential surface, a task beyond the scope of this study.

5 Discussion

The analysis of the PFI-ZEKE photoelectron spectrum presented in Section 4 leads to the conclusion that the vibrationless ground state of $C_2H_6^+$ has A_g or A_{1g} vibronic symmetry and rotational constants indicating a DB-like structure, which proves that the electronic ground state of $C_2H_6^+$ has A_g symmetry and confirms the result of *ab initio* calculations.

The spectrum also reveals the existence of at least two excited vibronic states of $C_2H_6^+$ within less than 600 cm^{-1} of internal excitation and which, accordingly to our analysis, have E_g vibrational symmetry. The nature of the vibrational excitation could, however, not be determined from the spectrum, and is now discussed in the context of the information obtained by EPR spectroscopy,^{20–22} *ab initio* calculations,^{7,9,10,13} and photoelectron spectroscopy.

According to *ab initio* calculations, the LB and DB isomers represent two distinct minima on the ground-state potential energy surface (A_g) of $C_2H_6^+$, as represented in Fig. 2. The red dots in Fig. 2 correspond to the results of a calculation of the A_{1g} state $(a_{1g})^{-1}$ obtained by constraining the molecular structure to D_{3d} symmetry. The comparison of the two curves shows that the LB isomer has an essentially pure $(a_{1g})^{-1}$ electronic configuration whereas the DB isomer has mixed $(a_{1g})^{-1}$ and $(e_g)^{-1}$ character, consistent with the analysis of the rotational structure of Band 1. Inspection of the optimized geometries along the dashed black line in Fig. 2 indicates a change of structure involving a substantial deformation of the methyl groups (DB-distortion modes) from the LB D_{3d} structure, where the coordinate is in good approximation a pure C–C stretching motion, to the DB structure. The nuclear motion of $C_2H_6^+$ at low energies is thus intrinsically multimodal and involves the DB distortion e_g modes, the C–C stretching mode, and, at large C–C distances, also the hindered internal rotation.

There are three equivalent D_{3d} LB structures connected by low internal-rotation barriers at large C–C distances (see Fig. 7b). There are also three equivalent DB structures connected by pseudorotational barriers at short C–C distance (see Fig. 7a).^{7,10} The latter barriers are known to be higher than the former.^{7,10}

The three equivalent DB configurations labeled b, b' and b'' in Fig. 8 of Ref. 7 and depicted schematically in Fig. 7a are connected by a large-amplitude motion that exchanges the pairs of labeled H atoms located on long C–H bonds from (1, 4) on the top panel to (2, 5) on the middle panel, and to (3, 6) on the bottom panel. The dynamics of the interconversion between these structures has been characterized by analysing the temperature dependence of the hyperfine structure of the EPR spectra.^{20–22} On the A_g potential, the electron-spin density corresponding to the DB structures depicted in Fig. 7a is primarily located on the two long, in-plane C–H bonds, which leads to an EPR triplet with hyperfine coupling constant of $\simeq 150 \text{ G}$ if the interconversion by pseudorotation does not take place on the experimental time scale, and to a septet with a three-times smaller hyperfine coupling constant if it does. Indeed, in this case, the spin density is equally shared by the six protons rather than by two protons only. If the interaction between $C_2H_6^+$ and the SF_6 matrix used in

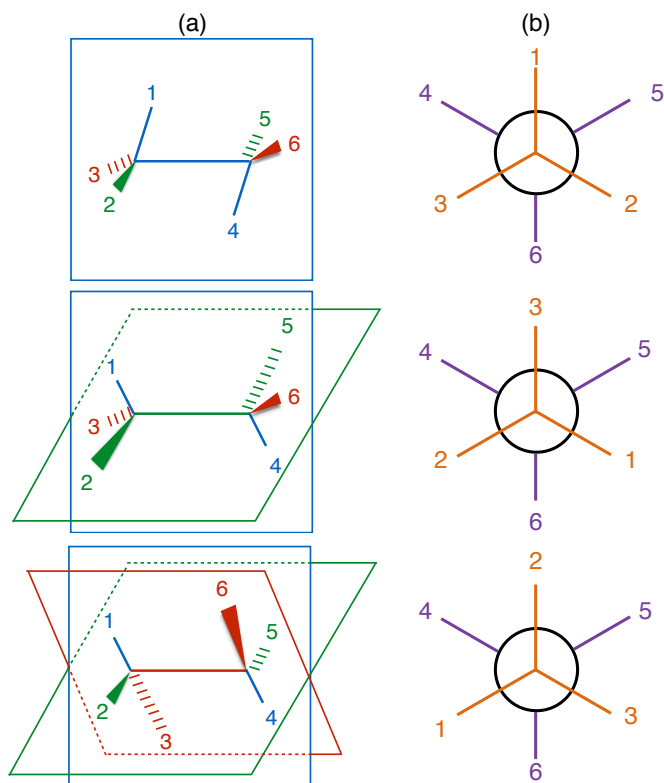


Fig. 7 Schematic representation of a) the three equivalent DB-like structures of $C_2H_6^+$ and b) the three equivalent LB structures of $C_2H_6^+$ connected by internal rotation.

the EPR experiments is assumed to be negligible, the EPR triplet observed at 4.2 K proves that the pseudorotational exchange of the protons does not occur in the ground state of $C_2H_6^+$. One cannot, however, exclude the possibility that the matrix suppresses the pseudorotation. The PFI-ZEKE photoelectron spectrum helps clarifying this ambiguity. A rapid pseudorotation of the isolated $C_2H_6^+$ molecules in the gas phase would necessitate the treatment of the rotational structure in the D_{3d} group and leads to a splitting of the ground state into an A_{1g} and an E_g component, which should both be observable in the photoelectron spectrum as a result of vibronic interactions. We only observe an A_g component and thus can rule out significant pseudorotational tunnelling on time scales faster than ~ 100 ps.

When the SF_6 matrix is held at 77 K, the EPR spectrum appears as a septet, which implies the equivalence of the six protons and a rapid interconversion of the three DB structures. The EPR spectrum is not the sum of a triplet and a septet contribution and one must conclude that the thermal excitation in the matrix induces the interconversion either by overcoming the transition states separating the C_{2h} minima or by causing rapid excitation to, and deexcitation from, excited vibronic states with wavefunctions delocalized over the C_{2h} minima.

The interconversion mechanism proposed in Refs. 7,10 on the basis of the relative energies of the stationary points of the A_g potential surface involves the reversible extension of the C–C bond, followed by internal rotation of the D_{3d} LB structures through low internal rotation barriers, which effectively renders all protons

equivalent. By providing information on the positions and symmetries of the low-lying vibronic states of $C_2H_6^+$, the PFI-ZEKE photoelectron spectrum also helps clarifying the interconversion mechanism.

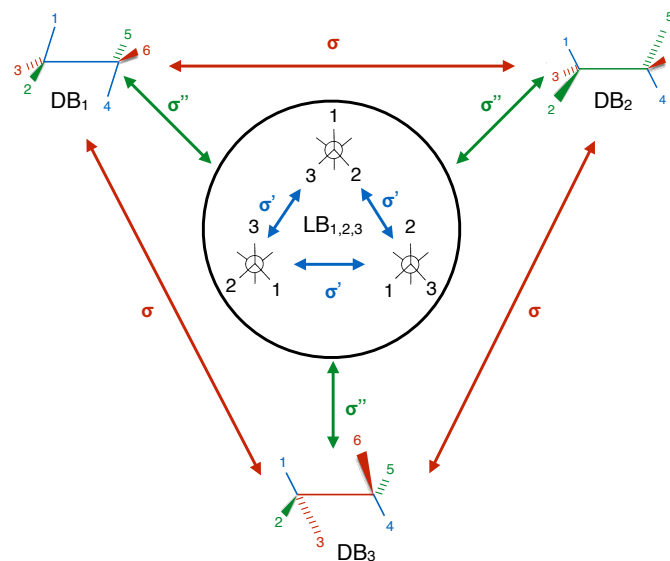


Fig. 8 Schematic representation of an effective coupling model to describe the interconversion between the three equivalent LB isomers and the three equivalent DB isomers of $C_2H_6^+$.

In analogy to the description of the fluxional behavior of CH_4^+ ,^{26,54} the interconversion model proposed for CH_4^+ in Ref. 29 can be expressed for $C_2H_6^+$ on the form of an effective tunnelling model represented schematically in Fig. 8. The three equivalent LB and the three equivalent DB structures are depicted at the edges of the inner (within the circle) and outer triangles, respectively, and the interconversion coupling elements σ , σ' and σ'' between the different structures are represented by double-sided arrows. The effective tunnelling model involves five parameters: the zero-order energy E_{DB} and E_{LB} of the DB and LB structures, which can be taken from high-level calculations (RCCSD(T)/VQZ-F12, see Section 3) of the potential energy along the C–C bond after correction for the zero-point vibrational motion; the pseudorotation coupling element σ , which interconverts the three equivalent DB structures; the internal-rotation coupling element σ' , which interconverts the three equivalent LB structures; and the coupling element σ'' , which interconverts the LB and DB structures. The effective tunnelling Hamiltonian corresponding to this model is

$$H_{ve} = \begin{pmatrix} E_{DB} & \sigma & \sigma & \sigma'' & \sigma'' & \sigma'' \\ \sigma & E_{DB} & \sigma & \sigma'' & \sigma'' & \sigma'' \\ \sigma & \sigma & E_{DB} & \sigma'' & \sigma'' & \sigma'' \\ \sigma'' & \sigma'' & \sigma'' & E_{LB} & \sigma' & \sigma' \\ \sigma'' & \sigma'' & \sigma'' & \sigma' & E_{LB} & \sigma' \\ \sigma'' & \sigma'' & \sigma'' & \sigma' & \sigma' & E_{LB} \end{pmatrix}. \quad (6)$$

Arbitrarily choosing the origin of the energy scale at $E_{DB} = 0$, fixing the value of E_{LB} to the value calculated *ab initio* ($E_{LB} = 250 \text{ cm}^{-1}$, see Section 3) and considering the pseudo-rotational

tunnelling to be negligible (i.e., taking $\sigma = 0$), in accord with the analysis of Band 1 and the conclusions reached in Refs. 7,10, the model involves only two parameters σ' and σ'' . The coupling elements σ' and σ'' can be taken as all having the same phase because of the significant PJT interaction, as explained in Refs. 29,55,56. Under these restrictions, the eigenvalues of Eq. (6) are

$$E_{1,6} = \frac{1}{2} \left(E_{\text{LB}} + \sigma' \mp \sqrt{36\sigma''^2 (E_{\text{LB}} + \sigma')^2} \right)$$

$$E_2 = E_3 = E_{\text{DB}} \quad (7)$$

$$E_4 = E_5 = E_{\text{LB}} - \sigma'$$

and include 2 nondegenerate (i.e., of A_{1g} vibronic symmetry) levels $E_{1,6}$ and two pairs of degenerate (i.e., of E_g vibronic symmetry) levels $E_{2,3}$ and $E_{4,5}$. With $\sigma' = 0.1 \text{ cm}^{-1}$, which corresponds to the internal-rotation barrier of 370 cm^{-1} calculated by Sulzbach *et al.*¹⁰ (CCSD(T)/TZ(2df, 2pd)) and taking the relative positions of Bands 1, 2 and 3 to correspond to the energies of E_1 , $E_{2,3}$ and $E_{4,5}$, the ionic levels observed experimentally can be reproduced qualitatively with a value σ'' of 160 cm^{-1} (see thick marks at the top of Fig. 3).

This model, though an obvious oversimplification of the vibronic dynamics, yields results that lend support to the interconversion mechanisms proposed in Refs. 7,10 and offers an interpretation of the first bands of the photoelectron spectrum that is compatible with the EPR spectrum and the results of *ab initio* calculations. The model also highlights the multimodal nature of the nuclear motion of C_2H_6^+ at low energies with large amplitude motions involving the C–C bond length, the internal rotation and the diborane distortion modes.

6 Conclusions

The study of the radical cation of ethane by high-resolution photoelectron spectroscopy and *ab initio* quantum chemistry presented in this article has enabled the characterization of several important aspects of its structure and dynamics related to the Jahn-Teller effect. The observation of several low-lying vibronic states indicated the importance of large-amplitude nuclear motion on a flat potential energy surface in the region of the two stable ground-state structures. The more stable of these two structures is diborane-like with C_{2h} point-group symmetry and lies energetically less than 5 kJ/mol below the other structure, which has an elongated C–C bond and D_{3d} point-group symmetry. From an analysis of the rotational structure of the photoelectron spectrum, the ground vibronic state of C_2H_6^+ was found to be diborane-like and have A_g electronic character with a mixed $(a_{1g})^{-1}$ and $(e_g)^{-1}$ electronic configuration. The rotational structures of the photoelectron spectra of the low-lying excited levels of C_2H_6^+ are complex and differ from that of the ground vibronic state. They indicate the importance of multimodal large amplitude motions in the dynamics of C_2H_6^+ . The new information obtained from the high-resolution photoelectron spectrum has been combined with the results of *ab initio* studies and earlier experimental studies of the photoelectron spectrum of C_2H_6 and EPR spectra of C_2H_6^+ in matrices in an effort to derive a consistent picture of the structure

and dynamics of C_2H_6^+ at low energies.

Acknowledgments

We thank Prof. K. Tanaka for useful discussions. This work is supported financially by the Swiss National Science Foundation under project Nr. 200020-172620.

References

- 1 N. Moazzen-Ahmadi, H. P. Gush, M. Halpern, H. Jagannath, A. Leung and I. Ozier, *J. Chem. Phys.*, 1988, **88**, 563–577.
- 2 I. B. Bersuker, *The Jahn-Teller effect*, Cambridge University Press, Cambridge UK, 2006.
- 3 *The Jahn-Teller effect*, ed. H. Köppel, D. R. Yarkony and H. Barntzen, Springer, Heidelberg, 2009.
- 4 A. Richartz, R. J. Buenker, P. J. Bruna and S. D. Peyerimhoff, *Mol. Phys.*, 1977, **33**, 1345–1366.
- 5 S. Lunell and M.-B. Huang, *J. Chem. Soc., Chem. Commun.*, 1989, 1031–1033.
- 6 M.-B. Huang and S. Lunell, *Chem. Phys.*, 1990, **147**, 85 – 90.
- 7 A. Ioffe and S. Shaik, *J. Chem. Soc., Perkin Trans. 2*, 1993, 1461–1473.
- 8 C. E. Hudson, D. J. McAdoo and C. S. Giam, *J. Comput. Chem.*, 1996, **17**, 1532–1540.
- 9 H. Zuilhof, J. P. Dinnocenzo, C. Reddy and S. Shaik, *J. Phys. Chem.*, 1996, **100**, 15774–15784.
- 10 H. M. Sulzbach, D. Graham, J. C. Stephens and H. F. Schaefer III, *Acta Chem. Scand.*, 1997, **51**, 547–555.
- 11 T. S. Venkatesan and S. Mahapatra, *J. Chem. Phys.*, 2005, **123**, 114308.
- 12 R. Kumar, T. Venkatesan and S. Mahapatra, *Chem. Phys.*, 2006, **329**, 76 – 89.
- 13 K. L. K. Lee, S. M. Rabidoux and J. F. Stanton, *J. Phys. Chem. A*, 2016, **120**, 7548–7553.
- 14 W. A. Lathan, L. A. Curtiss and J. A. Pople, *Mol. Phys.*, 1971, **22**, 1081–1088.
- 15 W. A. Lathan, W. J. Hehre, L. A. Curtiss and J. A. Pople, *J. Am. Chem. Soc.*, 1971, **93**, 6377–6387.
- 16 A. Richartz, R. J. Buenker and S. D. Peyerimhoff, *Chem. Phys.*, 1978, **28**, 305–312.
- 17 H. Köppel, W. Domcke and L. S. Cederbaum, *Adv. Chem. Phys.*, 1984, **57**, 59–246.
- 18 D. W. Turner, C. Baker, A. D. Baker and C. R. Brundle, *Molecular Photoelectron Spectroscopy: A Handbook of He 584 Å Spectra*, John Wiley & Sons, New York, 1970.
- 19 A. Baker, C. Baker, C. Brundle and D. Turner, *Int. J. Mass Spectrom. Ion Physics*, 1968, **1**, 285 – 301.
- 20 K. Toriyama, K. Nunome and M. Iwasaki, *J. Chem. Phys.*, 1982, **77**, 5891–5912.
- 21 M. Iwasaki, K. Toriyama and K. Nunome, *Radiat. Phys. Chem.*, 1983, **21**, 147 – 156.
- 22 M. Iwasaki, K. Toriyama and K. Nunome, *Chem. Phys. Lett.*, 1984, **111**, 309 – 314.
- 23 L. B. Knight Jr., G. M. King, J. T. Petty, M. Matsushita, T. Momose and T. Shida, *J. Chem. Phys.*, 1995, **103**, 3377–3385.

- 24 R. Signorell, M. Sommovilla and F. Merkt, *Chem. Phys. Lett.*, 1999, **312**, 139–148.
- 25 R. Signorell and M. Sommovilla, *J. Electron Spectrosc. Relat. Phenom.*, 2000, **108**, 169–176.
- 26 R. Signorell and F. Merkt, *Faraday Discuss.*, 2000, **115**, 205–228.
- 27 H. J. Wörner and F. Merkt, *J. Chem. Phys.*, 2007, **126**, 154304.
- 28 M. Grütter, H. J. Wörner and F. Merkt, *J. Chem. Phys.*, 2009, **131**, 024309.
- 29 H. J. Wörner and F. Merkt, *Angew. Chem. (int. ed. engl.)*, 2009, **48**, 6404–6424.
- 30 K. Müller-Dethlefs and E. W. Schlag, *Annu. Rev. Phys. Chem.*, 1991, **42**, 109–136.
- 31 M. I. Al-Joboury and D. W. Turner, *J. Chem. Soc. B*, 1967, 373–376.
- 32 A. D. Baker, D. Betteridge, N. R. Kemp and R. E. Kirby, *J. Mol. Struct.*, 1971, **8**, 75 – 81.
- 33 J. W. Rabalais and A. Katrib, *Mol. Phys.*, 1974, **27**, 923–931.
- 34 K. Kimura, S. Katsumata, Y. Achiba, T. Yamazaki and S. Iwata, *Handbook of HeI photoelectron spectra of fundamental organic molecules : ionization energies, ab initio assignments, and valence electronic structure for 200 molecules*, Japan scientific Societies Press, Tokyo, 1981.
- 35 P. Rupper and F. Merkt, *Rev. Sci. Instr.*, 2004, **75**, 613–622.
- 36 C. J. Sansonetti, J. Reader and K. Vogler, *Appl. Opt.*, 2001, **40**, 1974–1978.
- 37 U. Hollenstein, R. Seiler, H. Schmutz, M. Andrist and F. Merkt, *J. Chem. Phys.*, 2001, **115**, 5461–5469.
- 38 K. Andersson, P. Å. Malmqvist and B. O. Roos, *J. Chem. Phys.*, 1992, **96**, 1218–1226.
- 39 B. O. Roos, P. R. Taylor and P. E. M. Siegbahn, *Chem. Phys.*, 1980, **48**, 157–173.
- 40 K. Ruedenberg, M. W. Schmidt, M. M. Gilbert and S. T. Elbert, *Chem. Phys.*, 1982, **71**, 41–49.
- 41 H.-J. Werner and P. J. Knowles, *J. Chem. Phys.*, 1985, **82**, 5053–5063.
- 42 P. J. Knowles and H.-J. Werner, *Chem. Phys. Lett.*, 1985, **115**, 259–267.
- 43 F. Weigend and R. Ahlrichs, *Phys. Chem. Chem. Phys.*, 2005, **7**, 3297–3305.
- 44 T. B. Adler, G. Knizia and H.-J. Werner, *J. Chem. Phys.*, 2007, **127**, 221106.
- 45 G. Knizia, T. B. Adler and H.-J. Werner, *J. Chem. Phys.*, 2009, **130**, 054104.
- 46 P. J. Knowles, C. Hampel and H.-J. Werner, *J. Chem. Phys.*, 1993, **99**, 5219–5227.
- 47 P. J. Knowles, C. Hampel and H.-J. Werner, *J. Chem. Phys.*, 2000, **112**, 3106–3107.
- 48 K. A. Peterson, T. B. Adler and H.-J. Werner, *J. Chem. Phys.*, 2008, **128**, 084102.
- 49 H.-J. Werner, P. J. Knowles, G. Knizia, F. R. Manby and M. Schütz, *WIREs: Comput. Mol. Sci.*, 2012, **2**, 242–253.
- 50 F. Merkt, S. Willitsch and U. Hollenstein, *Handbook of High-Resolution Spectroscopy*, John Wiley & Sons, Chichester, 2011, vol. 3, p. 1617.
- 51 S. Willitsch and F. Merkt, *Intl. J. Mass. Spectrom.*, 2005, **245**, 14–25.
- 52 S. Dey, A. J. Dixon, I. E. McCarthy and E. Weigold, *J. Electron. Spectrosc. Relat. Phenom.*, 1976, **9**, 397 – 412.
- 53 R. A. Mackie, A. M. Sands, S. W. J. Scully, D. M. P. Holland, D. A. Shaw, K. F. Dunn and C. J. Latimer, *J. Phys. B: At. Mol. Opt. Phys.*, 2002, **35**, 1061.
- 54 H. J. Wörner, X. Qian and F. Merkt, *J. Chem. Phys.*, 2007, **126**, 144305.
- 55 G. Herzberg and H. C. Longuet-Higgins, *Discuss. Faraday Soc.*, 1963, **35**, 77–82.
- 56 F. S. Ham, *Phys. Rev. Lett.*, 1987, **58**, 725–728.